Computers and Structures 94–95 (2012) 54–69

Contents lists available at SciVerse ScienceDirect

Computers and Structures

journal homepage: www.elsevier.com/locate/compstruc

Investigation of a continuum damage model as an indicator for the prediction of spalling in fire exposed concrete

C.T. Davie *, H.L. Zhang, A. Gibson

School of Civil Engineering and Geosciences, Newcastle University, Newcastle upon Tyne, United Kingdom

ARTICLE INFO

Article history:
Received 24 October 2010
Accepted 14 December 2011
Available online 15 January 2012

Keywords:
Concrete
Fire
Spalling
Damage

ABSTRACT

Continuum damage theory has been widely adopted to model fracturing of concrete under mechanical loading and has been applied in capturing degradation of concrete under elevated temperatures. Here, the application of damage theory to prediction of concrete spalling in fire is investigated in the context of a fully coupled hygro-thermo-mechanical formulation. The ability of the model to capture spalling is assessed as is its sensitivity to choice of parametric relationships. The model, calibrated against experimental results, is shown to be a useful indicator for spalling. However, selection of model parameters must be carefully considered as a whole, not in isolation.

1. Introduction

Spalling is a common phenomenon observed when concrete elements are exposed to rapidly applied, elevated temperatures. It is, however, very difficult to accurately predict the development of spalling even using advanced numerical techniques. This is due to the complexity of the coupled hygro-thermo-mechanical-fracture behaviour involved in concrete exposed to elevated temperatures. Firstly, concrete is a multi-phase material, consisting of a porous solid skeleton, filled with liquid (and adsorbed) water and a mixture of gases, typically consisting of water vapour, and dry air. Most of its characteristic properties, such as intrinsic permeability, porosity, thermal conductivity, elasticity and strength, are temperature dependent and their initial values are often difficult to identify for a specific concrete. Secondly, when concrete elements are exposed to elevated temperatures, numerous complex phenomena will occur inside the concrete element, including heat conduction and convection, transport of liquid water and gases, evaporation of liquid water, dehydration of the cement paste and thermal expansion of the solid skeleton, some of which are strongly coupled with each other. These bring considerable challenges firstly in mathematically modelling these phenomena and secondly in developing a numerical solution for the problem due to its strong coupling and non-linearity. As a result of these difficulties, there are currently no models that can accurately predict the instant of the occurrence, the location and the extent of spalling.

In recent years, a number of mathematical formulations together with their numerical solutions have been developed for modelling of the coupled hygro-thermo-mechanical-fracturing behaviour of the concrete exposed to elevated temperatures, e.g. [1–4]. In these models, the continuum damage theory, firstly proposed by Mazars and Pijaudiercabot [5], has been widely adopted to model the fracturing or cracking of the concrete material. In continuum damage theory, a scalar between 0 and 1 is used to represent the severity of damage to the material, with 0 indicating intact material and 1 indicating complete damage. In this work it is considered that the development of damage, predicted by a model appropriately modified for thermal effects, can be used as an indicator for the development of thermal spalling.

In continuum damage theory, the fracture process is considered as a gradual, diffuse degradation of the material integrity. The concrete material is modelled as a continuum, but the stresses that can be transferred are assumed to decrease under the influence of mechanical, and in this case thermal, loading. Final fracture is represented by a zone in which the load-bearing capacity is completely lost. The development of the damage is determined by the equivalent strain measure and the damage evolution law. The equivalent strain measure determines the threshold for increment of the damage quantity, while the evolution law, which is characterised by a softening/hardening parameter, represents the global shape of the softening curve and the degree of brittleness of the response. Determination of these parameters in the damage model is therefore critical for prediction of the occurrence and evolution of damage. However, in relation to the existing models, there is a lack of detailed discussion on the selection of these parameters and their potential influences on the accuracy and reliability of numerical results and particularly with respect to the prediction of spalling.

* Corresponding author. Address: School of Civil Engineering and Geosciences, Drummond Building, Newcastle University, Newcastle upon Tyne NE1 7RU, United Kingdom. Tel.: +44(0)191 2226458.
E-mail address: colin.davie@ncl.ac.uk (C.T. Davie).

0045-7949
doi:10.1016/j.compstruc.2011.12.002

1.1. Scope of the work

For this work an existing numerical model for concrete exposed to elevated temperatures has been used [4]. The model employs of a fully coupled hygro-thermo-mechanical description as detailed in the following section. As part of the formulation a thermo-mechanical continuum damage model is included to capture the degradation of concrete resulting from both mechanical and thermal loading of the concrete. This is necessary to capture both the degradation of the mechanical properties and the coupled effects that are seen in the transport properties, such as permeability, porosity and conductivity.

The primary aim of this work was then to determine whether or not the damage predicted by this model under certain appropriate conditions can also be used as an indicator for the prediction of thermal spalling in concrete.

On consideration of the formulation of the damage criterion it can be seen that there are various components for which a choice can be made as to the constitutive or parametric behaviour of the concrete. These are primarily associated with the equivalent strain measure, the damage initiation threshold and the ductility of the concrete.

The second aim of this work was to determine the effects that the choice of these relationships has on the predicted development of damage, particularly with respect to thermal spalling behaviour as it has been observed in experimental and real cases.

2. Model formulation

In the mathematical formulation, concrete is treated at the macro-scopic level as a multiphase system consisting of solid, liquid and gas phases. The solid skeleton is assumed to develop isotropic elastic-damage deformations under mechanical and thermal loadings. The liquid phase consists of free liquid water in pores and adsorbed water physically bound to the surface of solid skeleton. The dehydrated water is considered as a part of free liquid water since chemically bound water is assumed to be initially released as liquid water. The gas phase is a mixture of dry air and water vapour, both of which are assumed to behave as ideal gases. Most of the material properties are variable (typically, either directly or indirectly, as a function of temperature). The complete description of the governing equations and material properties may be found in [4]. Herein, only a brief description is given of the governing equations and the transport equations. More detail is given of the mechanical constitutive equations and the damage model, which are the essential parts of the mathematical model in relation to this work.

2.1. Governing equations

The model consists of four governing equations (Eqs. (1)–(4)) defining the conservations of mass of dry air, mass of moisture (i.e., vapour and liquid), energy [6] and linear momentum [1], respectively.

$$\frac{\partial(\varepsilon_G\tilde{\rho}_A)}{\partial t} = -\nabla\cdot\mathbf{J}_A, \tag{1}$$

$$\frac{\partial(\varepsilon_G\tilde{\rho}_V)}{\partial t} + \frac{\partial(\varepsilon_L\rho_L)}{\partial t} - \frac{\partial(\varepsilon_D\rho_L)}{\partial t} = -\nabla\cdot(\mathbf{J}_V + \mathbf{J}_L), \tag{2}$$

$$(\underline{\rho C})\frac{\partial T}{\partial t} - \lambda_E\frac{\partial(\varepsilon_L\rho_L)}{\partial t} + (\lambda_D+\lambda_E)\frac{\partial(\varepsilon_D\rho_L)}{\partial t} = \nabla\cdot(k\nabla T) + \lambda_E\nabla\cdot\mathbf{J}_L, \tag{3}$$

$$\nabla\cdot(\sigma' - \eta P_{Pore}\mathbf{I}) + \mathbf{b} = 0, \tag{4}$$

where, ε_θ is the volume fraction of a phase $\theta(\theta = L,V,A,G,D$ refer to liquid water, water vapour, dry air, gas mixture and dehydrated water phases, respectively), ρ_θ is the density of a phase θ, $\tilde{\rho}_\theta$ the mass of a phase θ per unit volume of gaseous material, $\mathbf{J}_\theta$ the mass flux of a phase θ, $\underline{\rho C}$ the heat capacity of concrete, k the effective thermal conductivity of concrete, λ_E and λ_D are the specific heats of evaporation and dehydration, $\boldsymbol{\sigma}'$ is the Bishop's stress (also known as the effective stress in geomechanics), $\boldsymbol{I}$ he identity matrix, η is the Biot coefficient, P_{Pore} the pore pressure and $\boldsymbol{b}$ the body force.

2.2. Fluid transport equations

In the concrete, the liquid water flow is assumed to be driven by the pressure gradient under Darcy's law, while the gas flow is assumed to be driven by both the pressure gradient under Darcy's law and the concentration gradient under Fick's law. Therefore, the mass fluxes of dry air ($\boldsymbol{J_A}$), water vapour ($\boldsymbol{J_V}$) and liquid water ($\boldsymbol{J_L}$) per unit area of concrete are given by Eqs. (5)–(7).

$$\mathbf{J}_A = \varepsilon_G\tilde{\rho}_A\left(-\frac{k_g K K_G}{\mu_G}\right)\nabla P_G - \varepsilon_G\tilde{\rho}_G D_{AV}\nabla\left(\frac{\tilde{\rho}_A}{\tilde{\rho}_G}\right), \tag{5}$$

$$\mathbf{J}_V = \varepsilon_G\tilde{\rho}_V\left(-\frac{k_g K K_G}{\mu_G}\right)\nabla P_G - \varepsilon_G\tilde{\rho}_G D_{AV}\nabla\left(\frac{\tilde{\rho}_V}{\tilde{\rho}_G}\right), \tag{6}$$

$$\mathbf{J}_L = \varepsilon_L\rho_L\left(-\frac{K K_L}{\mu_L}\right)\nabla P_L, \tag{7}$$

where K is the intrinsic permeability of the dry concrete, K_θ, μ_θ and P_θ are the relative permeability, dynamic viscosity and pressure of the phase θ, k_g is the gas-slip modification factor and D_{AV} is the coefficient of diffusion for the dry air/water vapour mixture within the porous concrete.

2.3. Mechanical constitutive equations

The total strain ($\boldsymbol{\varepsilon}$) of the solid skeleton is considered to consist of elastic strain ($\boldsymbol{\varepsilon}^e$), free thermal strain ($\boldsymbol{\varepsilon}^{ft}$) and load induced thermal strain ($\boldsymbol{\varepsilon}^{lits}$), i.e.,

$$\boldsymbol{\varepsilon} = \boldsymbol{\varepsilon}^e + \boldsymbol{\varepsilon}^{ft} + \boldsymbol{\varepsilon}^{lits}. \tag{8}$$

The free thermal strain rate is calculated by way of Eq. (9):

$$\dot{\varepsilon}^{ft}_{ij} = \alpha\dot{T}\delta_{ij}, \tag{9}$$

where, α is a non-linear, temperature dependent coefficient of thermal expansion [4,7], $\dot{T}$ is the rate of temperature change and δ_{ij} is the Kronecker delta.

The load induced thermal strain rate is calculated as shown in Eq. (10):

$$\dot{\varepsilon}^{lits}_{ij} = \frac{\beta}{f^0_c}\left((1-v_c)\sigma'^{-}_{ij} - v_c\sigma'^{-}_{kk}\delta_{ij}\right)\dot{T} \quad \text{for } \dot{T} > 0, \tag{10}$$

where, β is the coefficient of load induced thermal strain, f^0_c is the initial compressive strength, v_c is the lateral component of the load induced thermal strain (similar to Poisson's effect) and σ'^{-}_{ij} is the negative (compressive) projection of the Bishop's stress tensor, σ'_{ij} [4,7].

2.4. Continuum scalar damage formulation

The fracture and the reduction of stiffness of the concrete are accounted for by an isotropic scalar damage model as described in the following, where a scalar damage parameter, Λ, is used to represent the failure state of the concrete, i.e. $\Lambda = 1$ indicating complete failure, while $\Lambda = 0$ indicates intact material. Assuming that the solid skeleton undertakes elastic-damage deformation and adopting the Bishop's stress concept, the stress–strain relationship can be written as:

$$\boldsymbol{\sigma}' = (1-\Lambda)\mathbf{D}_0 : \boldsymbol{\varepsilon}^e, \tag{11}$$

where $\boldsymbol{\sigma}'$ is the Bishop's stress, $\mathbf{D}_0$ is the initial elasticity tensor, and Λ is the scalar damage parameter, which can be further expressed as:

$$\Lambda = 1 - (1-\omega)(1-\chi), \tag{12}$$

where ω is the mechanical damage parameter, accounting for the loss of the elastic stiffness caused by the micro-fracturing of concrete that develops under loading and χ the thermal damage parameter, accounting for the reduction of the elastic stiffness due to thermally induced degradation of the cement paste.

The thermal damage parameter, χ, is defined as:

$$\chi = 1 - \frac{E(T)}{E_0}, \tag{13}$$

where E_0 is the elastic modulus at a reference temperature (normally 20 °C) [1].

The mechanical damage parameter, ω, is defined by a version of the Mazars type damage evolution law modified to account for thermo-mechanical behaviour [7]:

$$\omega = 1 - \frac{\kappa_0^{md}(T)}{\kappa^{md}}\left((1-\alpha) + \alpha e^{-\gamma(T)\left(\kappa^{md}-\kappa_0^{md}(T)\right)}\right), \tag{14}$$

where κ_0^{md}, which defines the threshold for the onset of damage, is a strain measure defined as the ratio of the tensile strength, $f_t(T)$, to the elastic modulus, $E(T)$, i.e.,

$$\kappa_0^{md} = \frac{f_t(T)}{E(T)}, \tag{15}$$

where $f_t(T)$ and $E(T)$ are both temperature dependent [7]. κ^{md} is the mechanical damage history parameter that records the maximum strain experienced to date and can be written as:

$$\kappa^{md} = \max\left\{\kappa_0^{md}, \max(\bar{\varepsilon})\right\} \tag{16}$$

where $\bar{\varepsilon}$ is a scalar mapping of the tensorial strain state known as the equivalent strain measure [8].

$\gamma(T)$ is the ductility parameter which controls the slope of the softening curve, representing the brittleness of the concrete, and is defined as:

$$\gamma(T) = l_c \frac{(1-\chi) f_t(T)}{G_f(T)}, \tag{17}$$

where G_f is the fracture Energy Release Rate and l_c is a proportionality factor that depends on the size of the localization zone and has units of length.

The term $(1-\alpha)$ represents the residual stress as $\omega \to 1$, expressed as a proportion of the original strength. For $\varepsilon \to \infty$ the stress approaches $(1-\alpha)E\kappa_0$ [8]. For simplicity in this work a value of $\alpha = 1$ has been adopted, i.e. the material is considered to have no residual strength.

2.5. Numerical solution

The governing equations are discretised in space using the standard finite element approximation, with the chosen primary variables of displacements, $\boldsymbol{u}$, temperature, T, gas pressure, P_G, and vapour content, $\tilde{\rho}_v$, and in time by a generalised mid-point finite difference scheme. Details of the formulation may be found in [4,6].

Finally, boundary conditions are defined for the primary variables. Temperature and vapour content are considered to obey Neumann type (flux) boundary conditions where energy and mass transport takes place across the boundary dependent on the conditions internal and external to the concrete. Gas pressure is considered to remain constant at the value of the atmospheric gas pressure.

2.6. Model validation

The model described here has been applied extensively to numerous problems ranging from isothermal drying, through problems related to the relatively slow heating of nuclear power plant structures, to problems related to rapid fire loading, such as those detailed in this work.

The validity of the model and its ability to accurately represent the multi-phase, macro-scopic behaviour of concrete exposed to elevated temperatures has been specifically demonstrated in [4] where it was applied to the analysis of two sets of experimental data produced by different authors.

3. Numerical investigations

3.1. Model problem and set up

As discussed above the scalar damage model employed in this work consists of a combination of two damage parameters, ω and χ, which respectively represent mechanical damage, due to stress, and thermal damage, representative of the material degradation observed on heating. The parameters are combined multiplicatively to compute the total damage [9,10]. However, where the thermal damage is in practice a diffuse phenomenon, occurring in correlation with the increased temperature field, the mechanical damage can be a more localised phenomenon and hence is considered here to be the most appropriate indicator for the development of cracking associated with spalling behaviour.

As also discussed previously, the mechanical damage formulation obeys a modified Mazars type criterion [7,8] as shown in Eq. (14). Taking into account the assumption of zero residual strength the formulation is simplified as shown below:

$$\omega = 1 - \frac{\kappa_0^{md}(T)}{\kappa^{md}} e^{-\gamma(T)\left(\kappa^{md}-\kappa_0^{md}(T)\right)}. \tag{18}$$

Within this formulation there are several components that are based on constitutive relationships describing in particular the temperature dependencies of the various parameters involved and for which a choice of relationship must be made. In the following sections the significance of the choices made are considered in relation to their effect on the results of analyses of two typical structural concrete problems in which spalling behaviour is often observed. These are namely a large concrete slab or wall and a square concrete column, both exposed to fire on all sides.

The wall exposed to fire on both sides was modelled as a one-dimensional problem in central-plane symmetry, as illustrated in Fig. 1 and the column exposed to fire on all sides was modelled as a two-dimensional problem in quarter-plane symmetry, as shown in Fig. 2.

Unless otherwise stated the basic material parameters for both problems were set as shown in Table 1.

These parameters are representative of typical concrete specimens and have been shown not to significantly affect the development of damage in these problems [11,12].

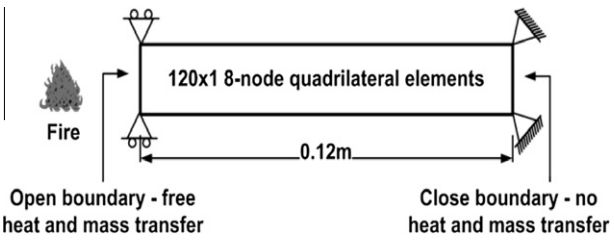

Fig. 1. Schematic diagram of model representing a concrete wall exposed to fire on both sides.

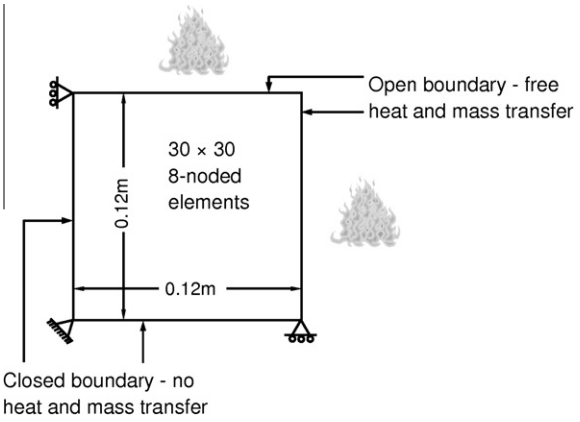

Fig. 2. Schematic diagram of model representing a concrete column exposed to fire on all sides.

Table 1
Initial parametric values used in all simulations.

Parameter	Symbol	Initial value
Internal temperature	T_0	293 K
Internal gas pressure	P_{G0}	0.1 MPa
Porosity	ϕ_0	12%
Young's modulus	E_0	30 GPa
Poisson's ratio	ν	0.2
Tensile strength	ft_0	3 MPa
Intrinsic permeability	K	1×10^{-19} m^2
Relative humidity	*R.H.*	65%
Thermal conductivity	k	1.95 W/m K

In all cases the heating due to fire is described by the standard ISO834 fire curve, as defined by Eq. (19).

$$T_\infty = 20 + 345\log_{10}(8t + 1) + 273.15, \tag{19}$$

where t is time in minutes.

For completeness results of temperature and pore pressure profiles for the two problems analysed in this work are shown below (Figs. 3 and 4).

These profiles are typical of such problems (e.g.[13,14]) and their validity is further supported by the work reported in [4]. It may be noted that they change very little throughout the analyses presented in this work since they are controlled by the thermal and mass transfer material properties as presented in Table 1. Minor changes may have occurred between analyses as a result of the coupling between the thermo-mechanical and hygro-thermal components of the model (i.e. for example changes in model parameters leading to changes in the development of damage, leading to changes in permeability, leading to changes in moisture transport, leading to changes in heat transport) however these have not been seen to be significant.

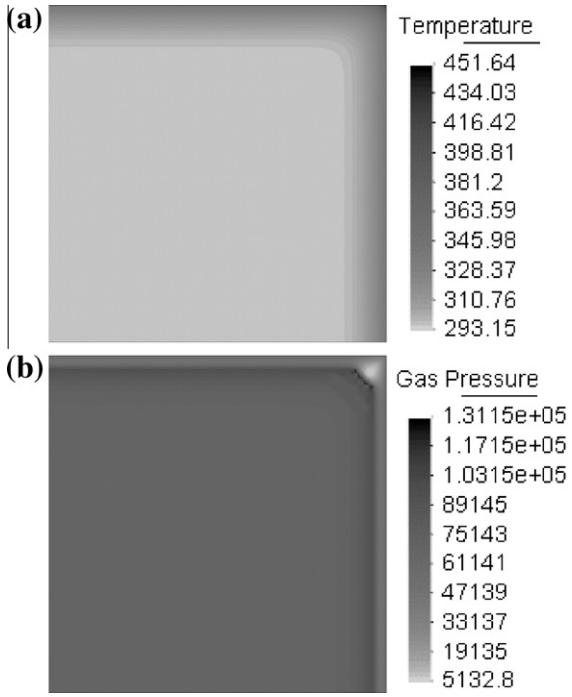

Fig. 4. Distributions of (a) temperature and (b) gas pressure in column problem after 210 s.

Furthermore, extensive parametric investigation has shown that although, as would be expected, variation of the thermo-mechanical properties (thermal conductivity, free thermal expansion, tensile strength, residual strength) does affect the specific results of these analyses, it does not affect the conclusions drawn from the studies carried out in this work. Further yet, the effects of pore pressure (as affected by the variation of porosity, permeability and moisture content) are specifically addressed in other work by the authors [11,12] and are not considered again here in detail. However, it may be noted that pore pressures do not influence the damage patterns seen in these analyses and as with the thermo-mechanical properties they do not affect the conclusions

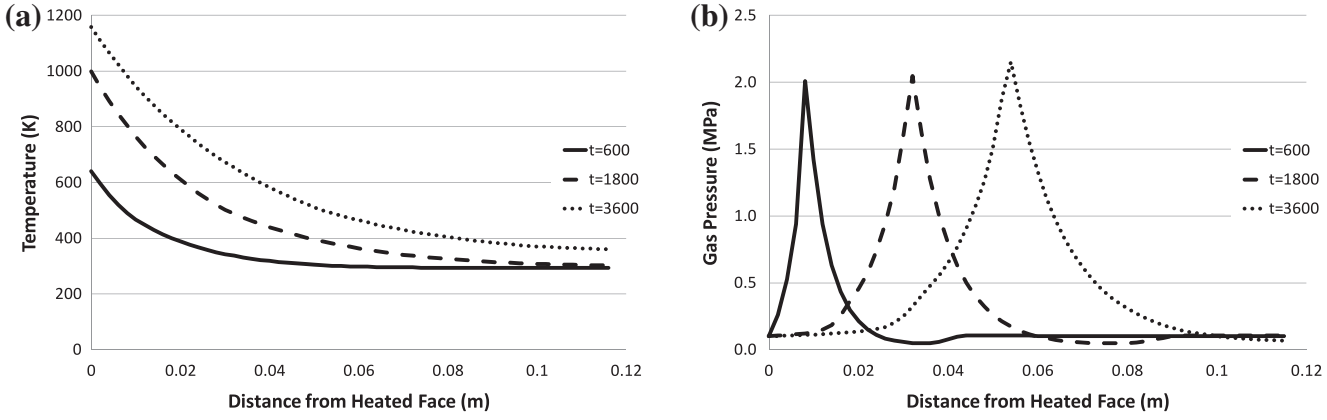

Fig. 3. Profiles of (a) temperature and (b) gas pressure in wall problem after 600 s, 1800 s and 3600 s.

of this work. The analyses presented in this work can therefore be considered representative of the general behaviour.

3.2. Equivalent strain measure

As described above and detailed in [7,8] mechanical damage is defined as occurring when the equivalent strain, which is a scalar mapping of the tensorial strain state, exceeds the mechanical damage history parameter κ^{md}, as described by Eq. (20)

$$\dot{\omega} \geqslant 0 \quad \text{if } (\bar{\varepsilon} - \kappa^{md}) = 0. \tag{20}$$

The equivalent strain mapping can be defined in numerous ways, as best represents the effects of the various strain components on the development of damage. Three typical formulations, which are commonly used to describe damage development in concrete both under normal and elevated temperature conditions (e.g. [10,15–22]), were considered by Peerlings et al. [8] in the context of direct tension and notched beam tests (under isothermal conditions). These same three are considered in this work to demonstrate the significance of the choice of formulation in the context of thermal spalling behaviour.

The formulations are shown below (21)–(23):

Energy Release Rate definition

$$\bar{\varepsilon} = \sqrt{\frac{1}{E}\boldsymbol{\varepsilon} : \mathbf{D} : \boldsymbol{\varepsilon}}. \tag{21}$$

Mazars definition

$$\bar{\varepsilon} = \sqrt{\sum_{i=1}^{3} \langle \varepsilon_i \rangle^2}, \tag{22}$$

where $\langle \varepsilon_i \rangle$ are the positive components of the principal strains.

Modified von Mises definition

$$\bar{\varepsilon} = \frac{g-1}{2g(1-2\nu)} I_1 + \frac{1}{2g}\sqrt{\frac{(g-1)^2}{(1-2\nu)^2} I_1^2 + \frac{2g}{(1+\nu)^2} J_2}, \tag{23}$$

where, I_1 is the first invariant of the strain tensor, J_2 is the second invariant of the deviatoric strain tensor, ν is the Poisson's ratio and g is the ratio of the compressive and tensile strengths.

Fig. 5 shows the predicted evolution of mechanical damage when these three equivalent strain measures are applied in the concrete wall problem. As can be seen three very different patterns of damage are produced.

Using the Energy Release Rate definition (Fig. 5a) the model predicts a very wide zone of damage and after 3600 s of exposure to fire the whole thickness of the wall is almost completely damaged. A similar but not quite so wide zone of damage is seen when the Mazars definition is applied (Fig. 5b). Neither of these patterns are particularly representative of the characteristically narrow zone of damage that is observed to occur near the fire exposed face during spalling (e.g. [13,23–25]). However, the pattern of damage predicted when the Modified von Mises definition is applied is much more representative of this behaviour. As can be seen in Fig. 5c the model predicts a sharply defined zone of damage that develops in the first 20–30 mm of the wall, very much in line with experimental observations.

These results are a function of the formulations and their sensitivity to the strain field developed as a result of the stress field, and particularly in the case of the wall problem, the development of strain as a result of tensile stresses. The strain in the wall problem is effectively 1-dimensional as the symmetry of the problem means that deformation (due to free thermal expansion) can only occur in the direction of the fire exposed face.

Similar behaviours are noted when the three formulations are applied to the column problem (Fig. 6). As can be seen, for the Energy Release Rate and Mazars definitions (Fig. 6a and b), large diffuse zones of damage are predicted starting from the heated surfaces. These do not correspond well with the typically observed phenomenon of corner spalling, where a fracture develops such that the corner of the column falls away, e.g.[26–29]. However, it may be noted in Fig. 6c that the pattern of damage predicted when the Modified von Mises definition is employed is again much more representative of this behaviour, with a narrow zone of damage forming across the corner.

These behaviours are again functions of the formulations and their sensitivity to the strain field and specifically a result of the

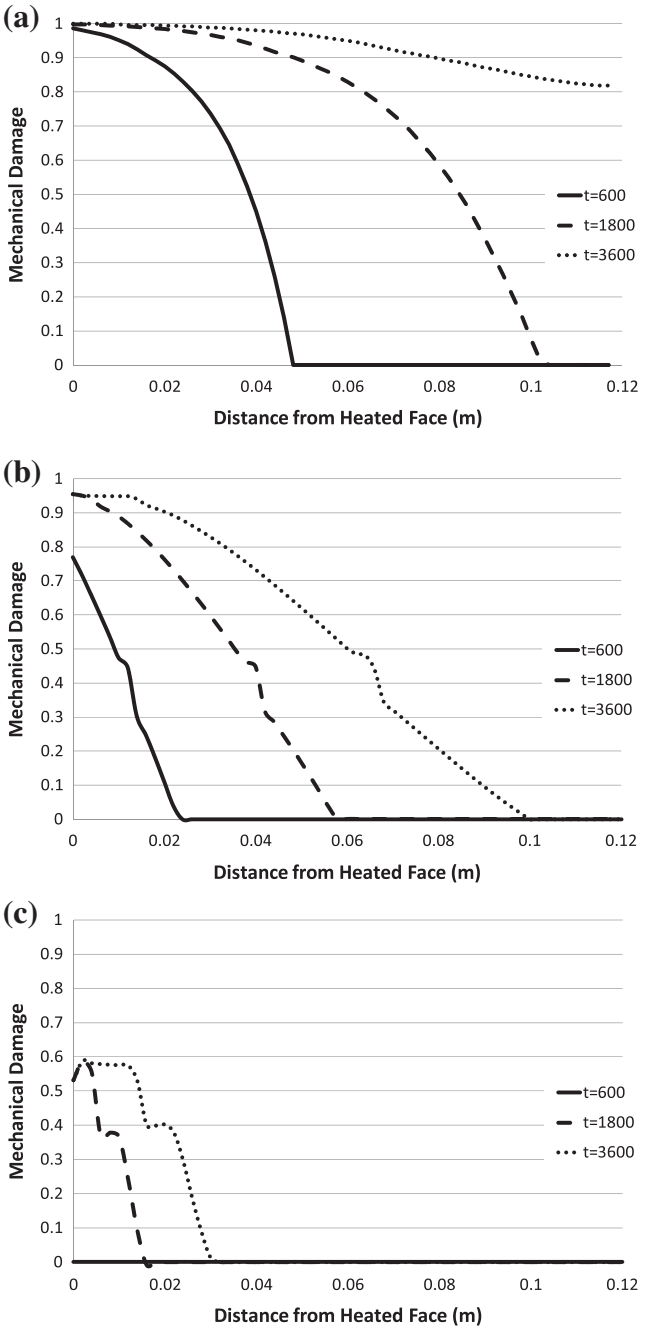

Fig. 5. Distributions of mechanical damage in wall problem after 600 s, 1800 s and 3600 s, with (a) Energy Release Rate, (b) Mazars type and (c) Modified von Mises equivalent strain definitions.

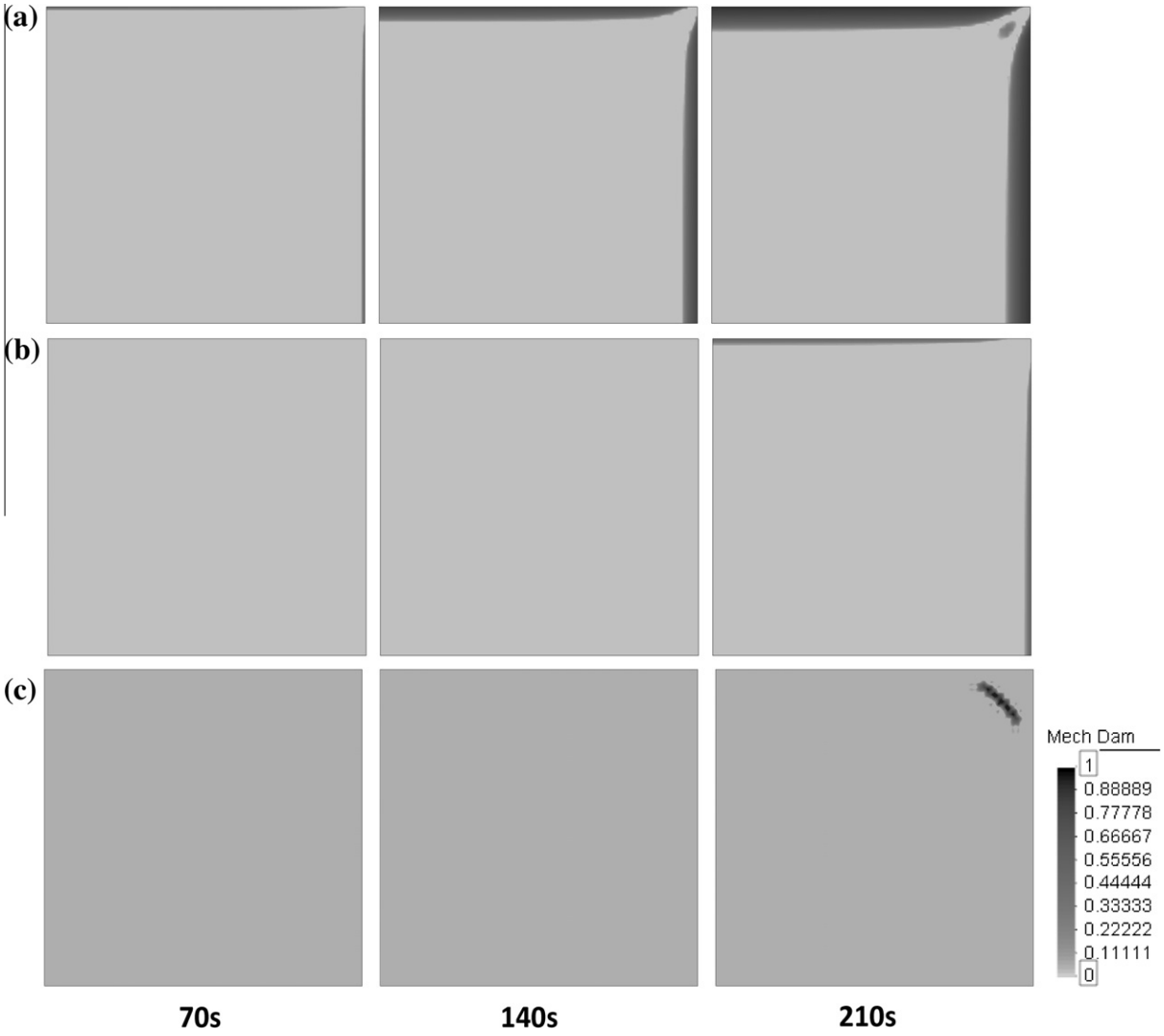

Fig. 6. Distributions of mechanical damage in column problem after 70 s, 140 s and 210 s, with (a) Energy Release Rate, (b) Mazars type and (c) Modified von Mises equivalent strain definitions.

ability of the formulations to distinguish between tensile and compressive behaviours and the relative roles that these appear to play in the development of thermally induced spalling. The Energy Release Rate definition treats tensile and compressive strains equally in terms of their capacity to cause damage; implying that the tensile and compressive strengths are the same. Large compressive stresses develop rapidly along the sides of the heated column resulting in large equivalent strains which, in the case of the Energy Release Rate definition, subsequently lead to the prediction of damage in these areas.

The Mazars definition does distinguish to some extent tensile and compressive behaviour and because of this, compressive effects have less influence and the zones of damage along the sides of the column are reduced from those developed by the Energy Release Rate definition. However, the weighting to the compressive behaviour that is inherent within the formulation is not sufficient to prevent the prediction of damage in the compressive areas of the column and the role of compressive behaviour is again apparently over estimated.

The Modified von Mises definition distinguishes between compressive and tensile behaviours much more than either of the other definitions by directly taking into account the ratio of the compressive and tensile strengths of the concrete (g in Eq. (23)). A value of 10, thought to be representative and typical of normal concrete, was employed by Peerlings et al. [8] and in this work. As can be seen in Fig. 6c this weighting meant that no damage was predicted in compressive areas of the column but a narrow band (a fracture) did form in the tensile region that develops due to the free thermal expansion of the corner diagonally outwards from the centre of the column. The similarity between this predicted behaviour and that observed in experimental works further suggests that spalling is primarily a function of tensile stresses (see also [11]).

It may therefore be concluded that the choice of equivalent strain formulation is extremely important in predicting the development of realistic patterns of damage and that, of the three tested formulae, the Modified von Mises definition gives results most closely representative of thermal spalling behaviour, due to its ability to capture the contributions of tensile and compressive behaviours representatively. This finding is in agreement with the findings of Peerlings et al. [8] in relation to tension dominant fracture behaviour in isothermal problems.

3.3. Modified von Mises strength ratio

As discussed in the previous section, the Modified von Mises definition of the equivalent strain measure (23) was shown to give

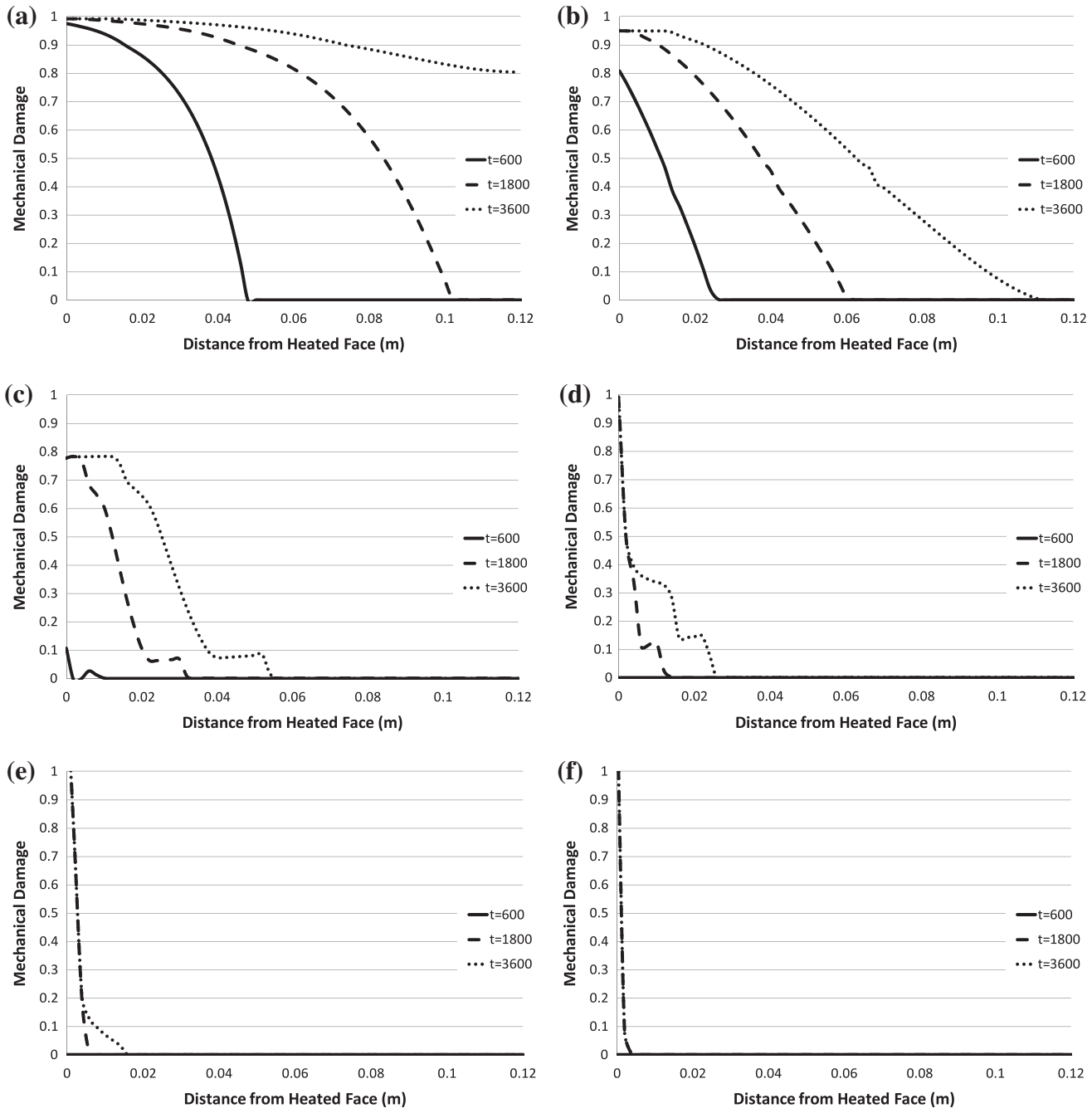

Fig. 7. Distributions of mechanical damage in wall problem after 600 s, 1800 s and 3600 s, with strength ratio g set to (a) 1, (b) 4, (c) 8, (d) 12, (e) 15 and (f) 20.

the best representation of observed spalling behaviour. This was in part due to its ability to distinguish between tensile and compressive behaviour which it does through the direct consideration of the ratio of the compressive to tensile strength of the concrete, g.

While a value of 10 was chosen for the work in the previous section (following [8]) and while this may be considered a reasonable assumption, it is clear that other values could be chosen and that in fact, since this is a parameter with physical meaning, values from experimental testing could be employed.

In this work analyses of wall and column problems have been carried in order to assess the influence of this parameter on the predicted results. Analyses were run as before with the value of g varied from 1 to 20. It should be noted that it has been considered reasonable in this work to assume that the compressive and tensile strengths degrade with temperature in the same way and hence the value of g remains constant throughout heating. Illustrative results are shown in Figs. 7 and 8.

As can be seen from Fig. 7 the value of g has a significant effect on the shape of the damage zone predicted in the wall problem. As the value is increased the zone becomes narrower towards the fire exposed face and arguably becomes more representative of observed spalling behaviour [13,23,24] with values of $g \geqslant 9$ appearing to be most appropriate. The results for $g = 1$ and $g = 4$ (Fig. 7a and b, respectively) are very similar to those seen in Fig. 5a and b for the Energy Release Rate (21) and Mazars (22) definitions and in fact it can be shown that the apparent weighting between compressive and tensile strengths for the those definitions are $g = 1$ and $g \approx 3.5$ (as reported in [8] for $\nu = 0.2$).

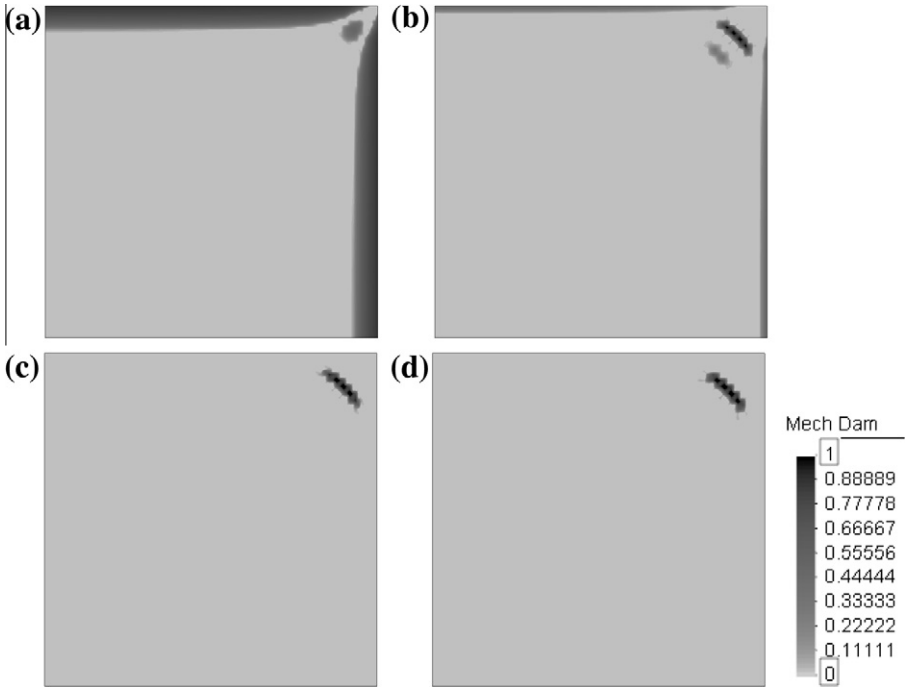

Fig. 8. Distributions of mechanical damage in column problem after 210 s, with strength ratio g set to (a) 1, (b) 4, (c) 7 and (d) 15.

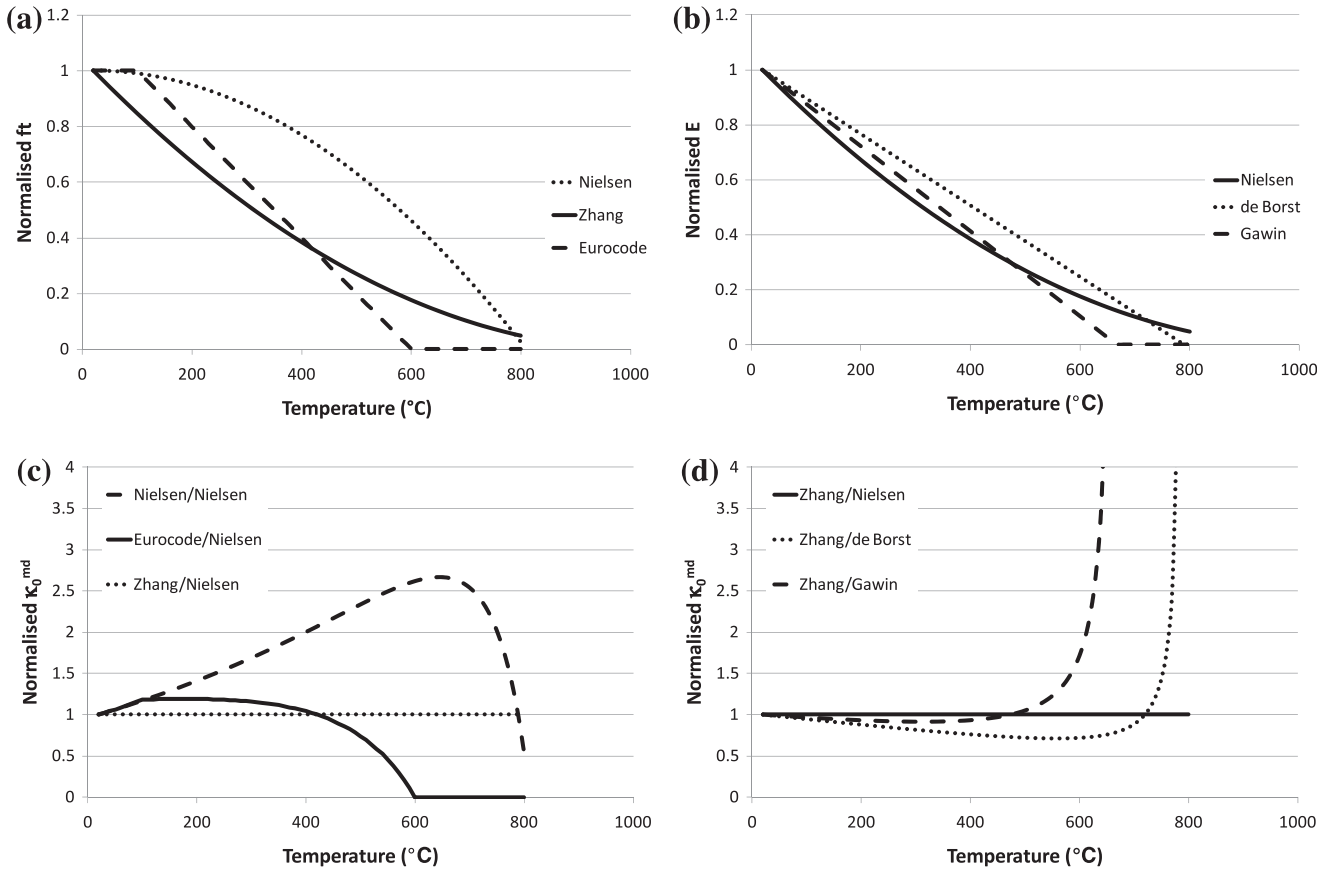

Fig. 9. Examples of normalised temperature dependent functions of (a) tensile strength [11,30,31], (b) elastic modulus [1,30,32], (c) damage initiation threshold using various $f_t(T)$ and (d) damage initiation threshold using various $E(T)$.

Again, similar behaviours are seen when the column problem is considered (Fig. 8). When a value of $g = 1$ is chosen (Fig. 8a), the results approach those predicted by the Energy Release Rate definition (Fig. 6a) and when a value of 4 is employed (Fig. 8b)

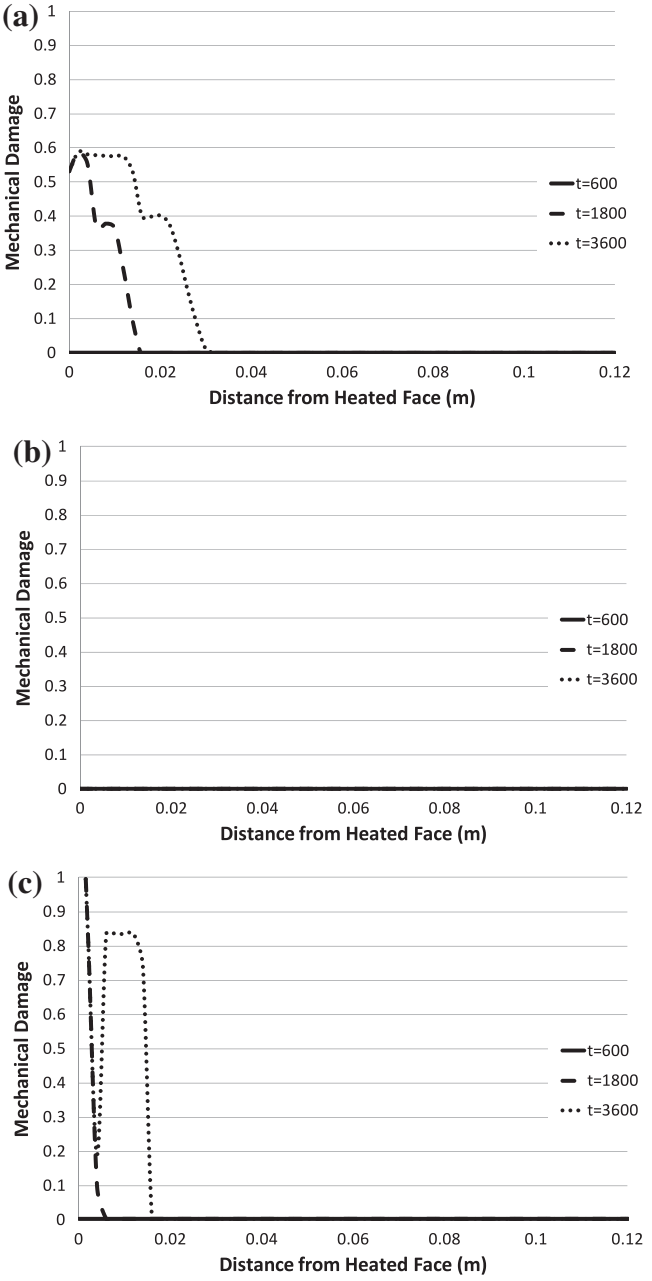

Fig. 10. Distributions of mechanical damage in wall problem after 600 s, 1800 s and 3600 s, with different ratios of $\kappa_0^{md} = f_t(T)/E(T)$ from Fig. 7c; (a) Zhang/Nielsen, (b) Nielsen/Nielsen and (c) Eurocode/Nielsen.

the results strongly resemble those of the Mazars definition (Fig. 6b). From Fig. 8c and d it may be noted that the results of the column problem are less sensitive to the magnitude of the strength ratio than those of the wall problem (Fig. 7). For values of $g \geqslant 7$ the predicted damage pattern is almost unchanged and tends to be representative of observed corner spalling behaviour, whereas the predicted damage pattern in the wall problem, although reasonably representative of observed behaviour, continued to change until a value of $g > 15$ was reached.

In considering the results above in terms of representative values for the strength ratio it is unlikely that values as low as 4 would occur in reality. This reinforces the findings of Section 3.2 which showed that, of the formulations tested, only the Modified von Mises definition of the equivalent strain was capable of differentiating between compressive and tensile effects sufficiently to accurately represent thermal spalling behaviour. It is also clear that, depending on the nature of the problem and particularly for cases where the ratio may be relatively low, it can be important to use the true value of g rather than an estimated value since this can have a significant effect on the results.

3.4. Damage initiation threshold

The damage initiation threshold, κ_0^{md}, is the ratio of the tensile strength to the elastic modulus of the concrete (15). When temperature effects are considered, as in this work, it must be noted that both the tensile strength and the elastic modulus are themselves temperature depend and both tend to decrease with temperature. Numerous constitutive functions may be found in the literature to describe the degradation of these properties with temperature and normalised versions of three typical examples of each are given in Fig. 9a and b below.

It can be seen that these functions have generally similar forms and it might therefore be considered that the choice of constitutive relationships for tensile strength and elastic modulus will have little effect on the overall behaviour predicted. Indeed this may be true when considering these properties in isolation. However, when the ratio κ_0^{md} is considered the choice of relationship has a much more significant effect.

Fig. 9c below shows normalised examples of κ_0^{md} as functions of temperature calculated using different tensile strength functions and the same the elastic modulus function. Similarly, Fig. 9d shows examples of κ_0^{md} calculated using different functions for the elastic modulus and the same tensile strength function. As can be seen, for only subtly differing input functions very different shapes are seen in the damage initiation threshold curves with some constant, some increasing and some decreasing with temperature.

By way of demonstrating the significance of these effects the three combinations of tensile strength and elastic modulus functions leading to the relationships shown in Fig. 9c were applied in the wall and column problems. The results are shown below in Figs. 10 and 11.

As can be seen in Fig. 10, the three different sets of relationships for $f_t(T)/E(T) = \kappa_0^{md}$ lead to the prediction of very different damage development. Fig. 10a are the 'original' results as shown in Section 3.2, which are considered to be a reasonable representation of the zone of damage observed in relation to thermal spalling behaviour; i.e. a narrow zone of intense damage near the fire exposed face of the concrete. In this case the ratio κ_0^{md} remained constant with increasing temperature as both the tensile strength, $f_t(T)$, and the elastic modulus, $E(T)$, were considered to degrade with temperature in the same way (Fig. 9c).

In contrast, when the second set of relationships was used, no damage was predicted to occur at all during exposure to the fire (Fig. 10b). This clearly does not represent observed spalling behaviour. As can be seen in Fig. 9c, this set of relationships produces a function for κ_0^{md} that increases with temperature up to ~650 °C before falling again, implying that it becomes increasingly more difficult to damage the concrete with increasing temperature. Considering the results shown in Fig. 10b, it would seem that functions of this type are not entirely representative of concrete behaviour under elevated temperatures or appropriate for the prediction of thermal spalling behaviour.

Fig. 10c shows the results when the third set of functions was employed. As with the first set, Fig. 10a, a narrow band of intense damage was predicted near to the fire exposed surface and arguably these results are even more representative of observed behaviour than the first set. In this case the function κ_0^{md} initially increases slightly before decreasing with increasing temperature, implying that overall it becomes easier to damage the concrete with increasing temperature. This function may well be most

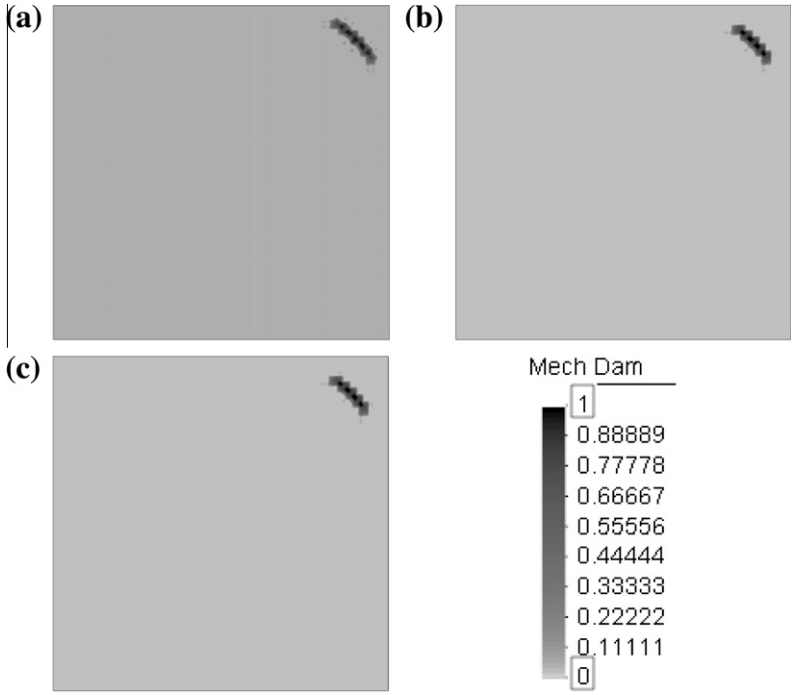

Fig. 11. Distributions of mechanical damage in column problem after 210, with different ratios of $\kappa_0^{md} = f_t(T)/E(T)$ from Fig. 7c; (a) Zhang/Nielsen, (b) Nielsen/Nielsen and (c) Eurocode/Nielsen.

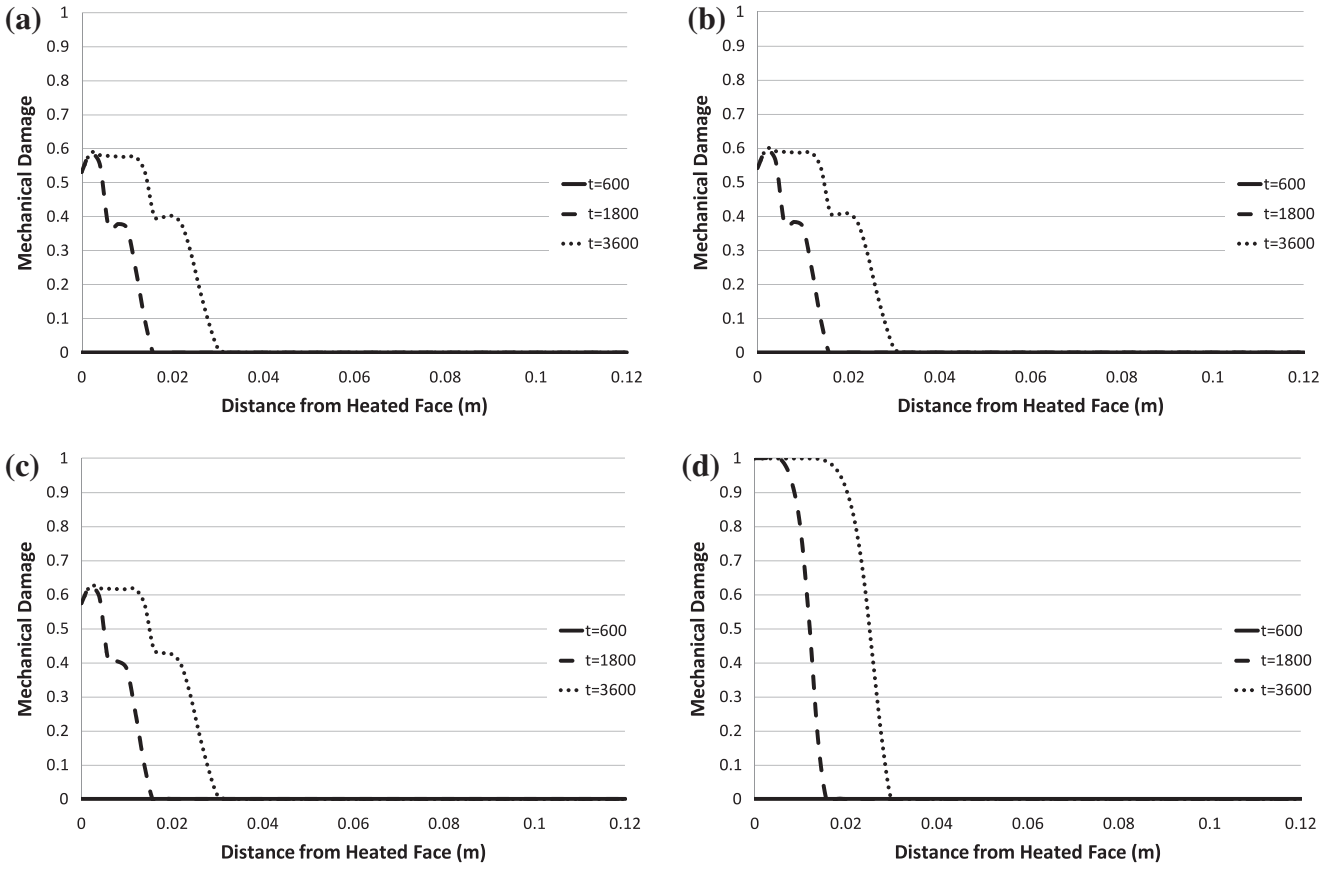

Fig. 12. Distributions of mechanical damage in wall problem after 600 s, 1800 s and 3600 s, with different ductilities: (a) original value, (b) 3 times original value, (c) 10 times original value and (d) 300 times original value.

representative of concrete behaviour as it could be considered to capture an initial increase in the concrete's resistance to failure due to continued hydration reactions in the cement paste, followed by a decrease as dehydration takes over at higher temperatures.

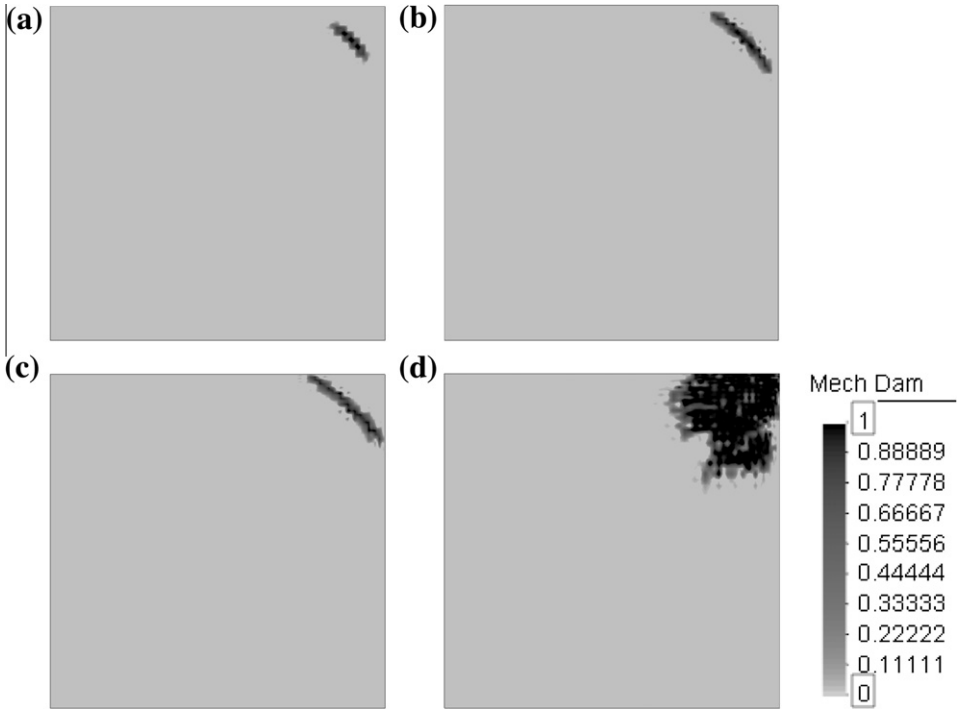

Fig. 13. Distributions of mechanical damage in column problem after 210 s, with different ductilities: (a) original value (b) 3 times original value, (c) 10 times original value and (d) 300 times original value.

However, it may also be noted that the Eurocode function for concrete strength [31] employed in this analysis is anecdotally considered by some researchers in the field to be overly conservative. Nonetheless, a similar form of decreasing function, or at least a constant function for κ_0^{md}, may be most appropriate.

Fig. 11 shows the results of the column problem when the same three sets of functions for $f_t(T)/E(T) = \kappa_0^{md}$ were employed. In this case it can be seen that all three analyses produced results considered to be representative of corner spalling, as discussed in Section 3.2. It can also be seen that there was very little difference between the three sets of results and although there was a slightly larger zone of damage development predicted for the first set of functions (Fig. 11a), the second and third sets produced almost identical results (Fig. 11b and c).

Initially this may seem contrary to the findings of the wall problem. However, upon inspection of the temperature fields it was found that, at the point of damage initiation, the concrete was experiencing relatively low temperatures of approximately 70 °C. Comparing the three ratios of κ_0^{md} as functions of temperature (Fig. 9c), it can be seen that, although the functions diverge significantly at higher temperatures, in the region of 70 °C the functions are very similar, and the second and third functions are overlain. The results produced are thus very similar, with the first (constant) function of κ_0^{md} predicting slightly more damage because it has not increased as the other two functions have.

Thus the findings related to the wall problem, where long exposures to higher temperatures were experienced, may not be so significant for problems where shorter exposures and lower temperatures are experienced.

3.5. Ductility

The final parameter for which a choice of value or constitutive relationship is available is the ductility of the concrete, γ. There are a number of levels of complexity that can be considered with respect to representation of the ductility parameter and its influence on the development of damage. In this section two implementations will be examined in turn and the significance of the choice will be considered in relation to the wall and column problems as before.

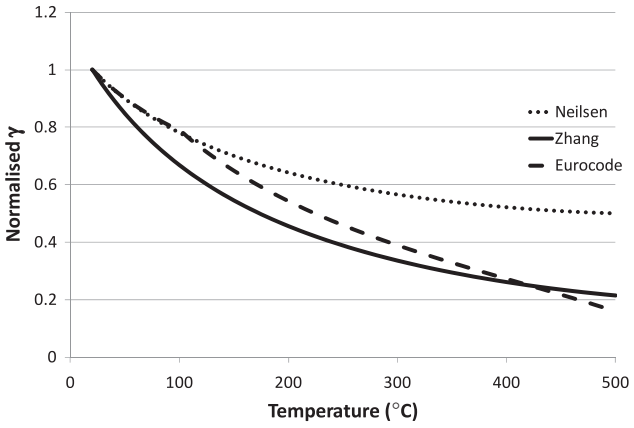

Fig. 14. Examples of normalised temperature dependent functions of ductility using various $f_t(T)$ from [11,30,31].

The first description is simply as a constant value representative of the ductility or brittleness of the concrete under consideration. The parameter has no real physical meaning on its own and is dimensionless. The higher the value of γ, the more brittle the concrete is. In the first set of analyses the basic effects of the ductility parameter are demonstrated by increasing its value over three orders of magnitude. Representative results are shown in Figs. 12 and 13 for the wall and column problems.

As can be seen in Fig. 12 the results of the wall problem are relatively insensitive to the ductility. Increasing the ductility parameter up to 10 times the original value (Fig. 12b and c) has very little effect on the predicted zone of damage, with only a very slight increase in the magnitude of damage caused. It is only when the magnitude of the ductility parameter is increased by a relatively

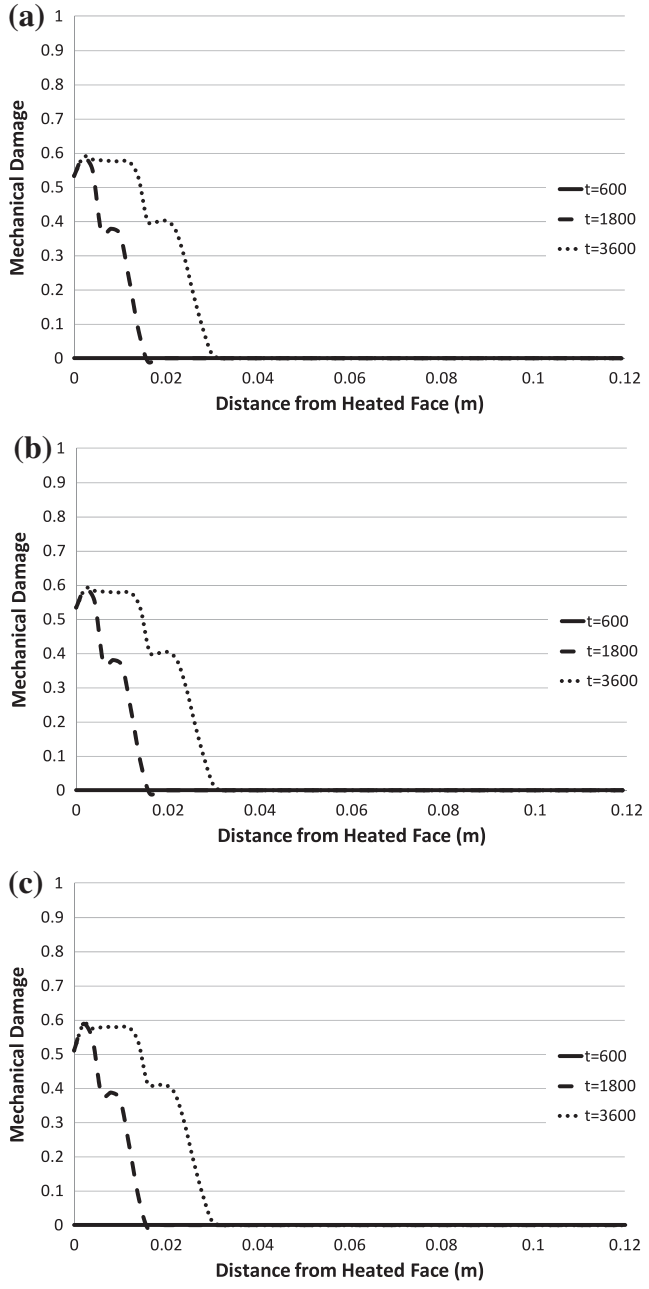

Fig. 15. Distributions of mechanical damage in wall problem after 600 s, 1800 s and 3600 s, with different ductility functions $\gamma(T)$ from Fig. 12; using $f_t(T)$ of (a) Zhang, (b) Nielsen and (c) Eurocode. κ_0^{md}constant for all analyses.

large amount, on the order of hundreds of times its original value, that a marked difference in the results is seen (Fig. 12d). At this point the predicted damage zone has become much larger in magnitude, and although it remains as a narrow band close to the fire exposed surface, once initiated it forms relatively rapidly, which is to be expected for an increasingly brittle material. Arguably, as the ductility parameter is increased, the predicted damage behaviour becomes more representative of observed thermal spalling behaviour. However, it is also clear that, if it is possible to relate the ductility parameter to real material parameters then a realistic representation of ductility parameter is desirable.

Fig. 13 shows the results when the same ratios of the ductility parameter as were applied in the wall problem are applied in the column problem. As can be seen this problem seems to be more sensitive to the ductility parameter than the wall problem. As the value of the parameter is increased, and the brittleness is increased, the predicted damage zone becomes increasingly extended towards the edges of the column (Fig. 13a–c). Again this is as would be expected for an increasingly brittle material and the rate of growth of the damage zone also increases. As the damage zone extends towards the edges of the column the behaviour becomes more representative of observed corner spalling behaviour where a piece of material is freed by formation of a fracture to fall away from the column, e.g. [26,28]. However, it must again be acknowledged that a value for the ductility parameter that is representative of the concrete's true material properties should be found.

A different behaviour is seen in Fig. 13d when the ductility parameter has been increased by hundreds of times its original value. As can be seen a relatively large and diffuse zone of damage is formed that no longer has the distinctive shape indicative of a fracture. It may also be noted that similarly to the results for the wall problem seen in Fig. 12d this zone of damage forms almost instantaneously after initiation. While this behaviour may be partly an artefact of the numerical formulation it may also go some way to suggesting an underlying behavioural change to explosive spalling [33].

Rather than choosing a fixed value for the ductility parameter, a way to relate the ductility to the true material properties of the concrete may be found using the temperature dependent formulation shown in Eq. (17). As can be seen, the parameter, which controls the slope of the softening curve, is a function of the tensile strength of the concrete, $f_t(T)$, and the fracture Energy Release Rate, $G_f(T)$, both of which are functions of temperature. As with the damage initiation threshold considered in the previous section, this allows the possibility of selecting parametric relationships from the literature. By way of example three sets of analyses have been conducted using different functions for the tensile strength, $f_t(T)$, as in the previous study (Section 3.4). It should be noted that in order to isolate the temperature dependent effects of the ductility relationship in these analyses, the damage initiation threshold, κ_0^{md}, was held constant (see Eq. (15)).

Fig. 14 shows three normalised temperature relationships for the ductility using different temperature dependent functions for the tensile strength, $f_t(T)$. As can be seen, significant differences in the ductility behaviour are described.

Fig. 15 shows the results of the wall problem when these three relationships are employed. As can be seen very little effect was noted between these analyses and furthermore very little difference was seen to the results where a constant ductility was employed; comparing Fig. 15a with Figs. 5c and 12a. This implies that, although the initial value of the ductility parameter is extremely important in controlling the development of damage and its correspondence to observed spalling behaviour, the development of ductility with temperature is much less important.

Very similar behaviour is seen in the results of the column problem, where, as can be seen in Fig. 16, the temperature dependence of the ductility has almost no effect on the predicted pattern of damage.

It is noted that, in addition to the main fracture like zone of damage, a very small patch of damage appears close to the corner of the column in all three of these analyses. This then appears to be a small difference to the behaviour when ductility is held constant with temperature; see Fig. 13a. However, upon further examination it is found that this patch of damage also occurs when the ductility parameter is held constant, but at a slightly later time in the analysis and is a result of the temperature dependent ductility changing the stress state slightly from that developed under constant ductility. This is therefore not considered to be a significant difference in behaviour.

What has not been considered here is the effect of the temperature dependent relationship for the fracture energy, $G_f(T)$. Clearly,

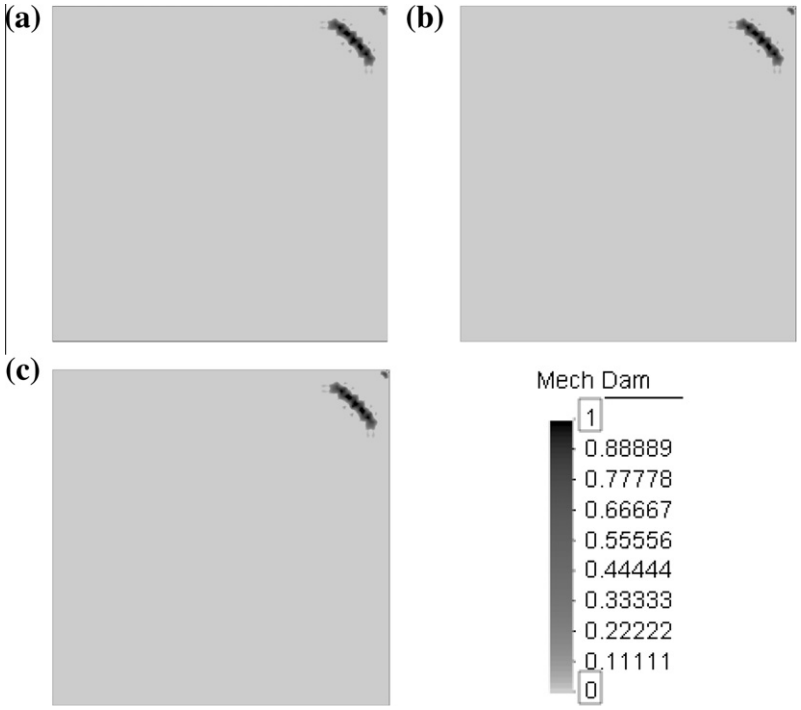

Fig. 16. Distributions of mechanical damage in column problem after 210, with different ductility functions $\gamma(T)$ from Fig. 12; using $f_k(T)$ of (a) Zhang, (b) Nielsen and (c) Eurocode. κ_0^{md} constant for all analyses.

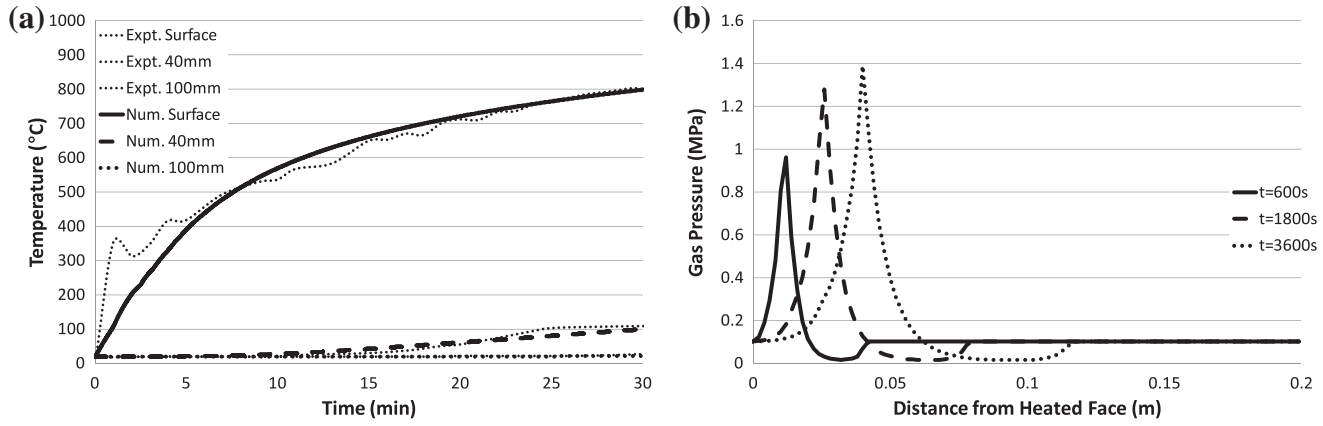

Fig. 17. (a) Comparison of numerical and experimental temperature development in time at depths of 0 mm, 40 mm and 100 mm and (b) numerical predictions of gas pressure profiles after 600 s, 1800 s and 3600 s.

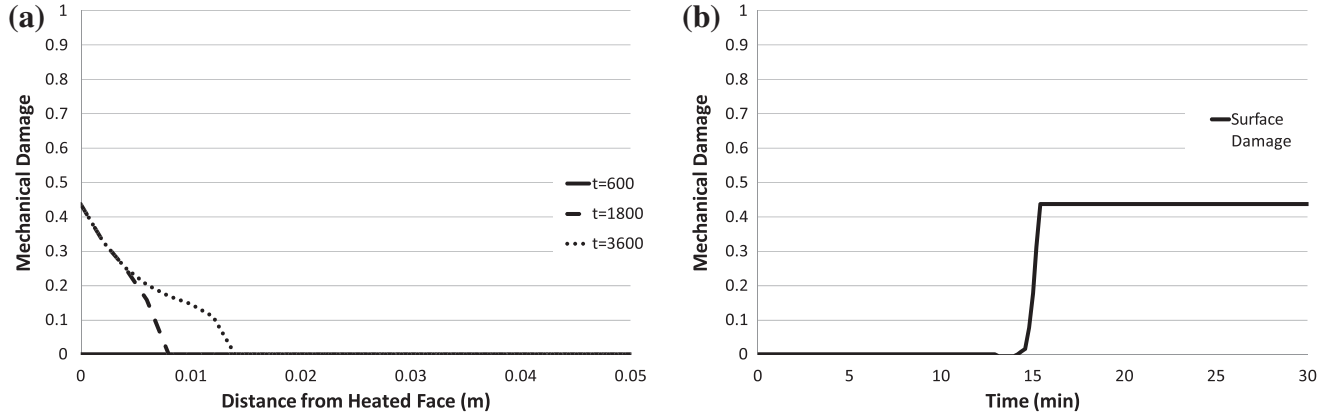

Fig. 18. (a) Distributions of mechanical damage in Ali slab problem after 600 s, 1800 s and 3600 s and (b) development of damage in time.

Table 2
Calibrated damage model parameters.

Parameter		Initial value
Equivalent strain measure	$\bar{\varepsilon}$	Modified von Mises
Compressive/tensile strength ratio	$g = f_c(T)/f_t(T)$	10
Damage initiation threshold	$\kappa_0^{md} = f_t(T)/E(T)$	$f_t(T)$ – Zhang/E (T) – Nielsen constant with temperature
Ductility measure	$\gamma(T) = \gamma(f_t(T))$	$f_t(T)$ – Zhang temperature dependent function of tensile strength and fracture energy

this offers yet a further opportunity where a choice of relationship may be made and the variance of ductility with temperature will be affected. The relationship for $G_f(T)$ used here follows the work of Pearce et al. [7] and although investigations of the temperature dependence of the fracture energy of concrete are limited some other relationships may be found, e.g. [34,35]. However, given the findings above it seems unlikely that the choice of fracture energy relationship will have a significant effect on the predicted pattern of damage.

What is of more interest is the initial value of ductility calculated from the ratio of tensile strength over fracture energy (Eq. (17)). The first set of ductility analyses above (Figs. 12 and 13) showed that higher values of the ductility parameter (increased brittleness) produced the best representation of observed spalling behaviour and it therefore seems logical to tune a constant value of ductility to produce the desired behaviour in the model. However, taking realistic values of initial tensile strength and fracture energy (which are measurable material properties), a relatively low value of the ductility parameter is produced, similar to the 'original values' employed in the analyses above (see Figs. 12 and 11). It is not yet clear how these two slightly contradictory observations can be rationalised although it may be noted that Eq. (17) also contains a proportionality factor, related to the size of the localisation zone, which could be used to tune the behaviour. Nonetheless, the benefits of using realistic functions for tensile strength and fracture energy within the ductility term are not clear for the problems considered in this work and, although more work is required, it may be better to simplify the model and neglect these terms.

3.6. Model calibration

The parametric studies above give insight into the thermo-mechanical behaviour of concrete at high temperatures and into the sensitivities of the damage formulation with respect to temperature and in the context of spalling.

In order to apply the model to real cases it is desirable to calibrate the model parameters. To achieve this the wall model (Fig. 1) was modified to represent the experimental work reported by Ali et al. [25], which considered large slabs exposed to the ISO834 fire curve (Eq. (19)) on one side.

The thermo-mechanical parameters were first tuned to give the best match with the reported temperature results (Fig. 17a). Results of gas pressures were not reported by Ali et al. but numerical results have been included for completeness and demonstrate that the behaviour is typical of such problems (Fig. 17b).

The damage parameters were then tuned to give the best match with the reported spalling behaviour, which was observed to initiate between 15 and 16.5 min after the start of heating and to reach depths between 15 and 25 mm. Fig. 18a and b show the numerical predictions for the development of damage in time.

As can be seen both the distribution of damage and the time of damage initiation match well with the reported results. The calibrated model parameters are shown in Table 2.

Equivalent strain measure – The Modified von Mises measure was found to give the most appropriate damage profiles, with both the Energy Release Rate and Mazars measures predicting damage almost from the beginning of heating and to too great a depth.

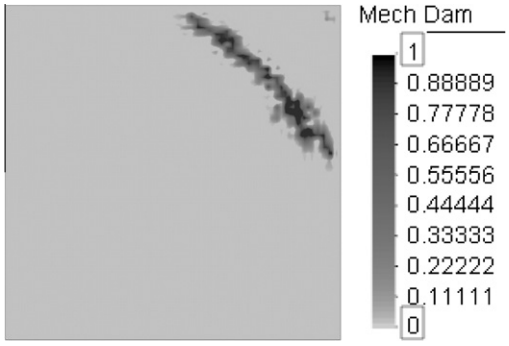

Fig. 19. Distributions of mechanical damage in Kodur column problem after 280 s.

Compressive to tensile strength ratio – A ratio below 10 decreased the depth to which damage developed. A ratio above 10 made little difference to the results. Without further information reported in the experimental data, a value of 10 was felt to be most appropriate.

Damage initiation threshold – Using the Eurocode function for tensile strength decreased the depth to which damage developed. Using the Nielsen function for tensile strength produced no damage at all. A constant value for the damage initiation threshold, using the Zhang function for tensile strength, was therefore found to be most suitable.

Ductility – Increasing the ductility parameter by up to 10 times its original value made little difference to the results. Continuing to increase the parameter initially tended to reduce the depth of the damage that developed and latterly resulted in the damage initiating too early. The original, temperature dependent function was therefore determined to be most appropriate.

These findings are consistent with those of the parametric studies reported above.

As a further check, the calibrated damage model was then similarly applied to a corner spalling problem representative of the experimental work of Kodur and McGrath [29]. The predicted damage distribution is shown in Fig. 19.

These results are qualitatively a good match for those described by Kodur et al., with a crack developing across the corner of the column at a depth of approximately 40 mm, which could ultimately allow a piece to fall freely from the corner and thus spalling to occur, and hence further confirm the calibration of the model. Unfortunately, continuation of the analysis was prevented by numerical instability resulting from locally high levels of damage. However, in further support of these findings, similar patterns of damage were also reported independently by Fu and Li [36].

4. Conclusion

This work has shown that the damage model employed within the formulation of the hygro-thermo-mechanical model to capture the mechanically and thermally driven degradation of the material, and to subsequently capture the coupled effects on transport behaviour, can also inherently capture thermal spalling behaviour

if the appropriate constitutive and parametric relationships are employed. The model was shown to predict damage development in areas and patterns, and at times, strongly representative and indicative of observed spalling behaviour.

In considering the selection of constitutive and parametric relationships it was particularly noted that the choice of equivalent strain measure was essential in predicting patterns of damage that occur in the tensile regions of the concrete members and hence capture observed spalling behaviour. Of the formulations examined in this work a Modified von Mises criterion was found to be most appropriate due to its ability to distinguish the behaviour of the concrete relative to the tensile and compressive strengths of the material. The Energy Release Rate and Mazars criteria were not found suitable for the prediction of thermal spalling.

Where the Modified von Mises criterion was employed it was also found that the precise value of the ratio of the tensile to compressive strength was important and it is recommended that the true value rather than a typical value should be employed wherever possible. Further consideration might also be given as to how this ratio changes with temperature but a constant value was considered acceptable here.

The development of the damage initiation threshold with temperature was also found to be critical to the prediction of the damage pattern in the concrete and parametric functions that were constant with temperature or that decreased with temperature were most appropriate. More importantly, since these functions depend on the ratio of the tensile strength to the elastic modulus, the choice of temperature dependent functions for these two parameters was most important. While these functions must clearly represent the appropriate effects of material degradation, as is variously recorded in the literature, they should not be considered in isolation. The simplest formulation for these parameters would consider them both to degrade in the same way with temperature and hence the damage initiation threshold to remain constant with temperature. Since this was shown to give reasonable results in relation to observed spalling behaviour this may be recommended practice.

Finally it was found that, although perhaps not as significant as the other parameters, the ductility of the material is important in refining the pattern and rate of damage development and hence its relationship to observed spalling behaviour. Higher values of the ductility parameter (increased brittleness) were found to give best results, and very high values may help to explain explosive spalling behaviour. However, it was also found to be difficult to relate the need for high values of the ductility parameter to the strongly related material properties of tensile strength and fracture energy. It may be possible to tune the ductility parameter using the associated proportionality factor, which is related to the size of the localisation zone, and further work is required in this area. However, since little effect was seen on the results when using temperature dependent functions for ductility, it may be simplest at present, to select an appropriate constant value for ductility.

Acknowledgements

This work was carried out as part of a research project (ep/e048935/1 – an advanced numerical tool for the prediction and analysis of spalling in concrete structures exposed to combined thermal and mechanical loading) funded by the engineering and physical sciences research council (epsrc), UK.

References

[1] Gawin D, Majorana CE, Schrefler BA. Numerical analysis of hygro-thermal behaviour and damage of concrete at high temperature. Mech Cohesive-Friction Mater 1999;4:37–74.
[2] Witek A et al. Finite element analysis of various methods for protection of concrete structures against spalling during fire. Comput Mech 2007;39(3):271–92.
[3] Tenchev R, Purnell P. An application of a damage constitutive model to concrete at high temperature and prediction of spalling. Int J Solids Struct 2005;42(26):6550–65.
[4] Davie CT, Pearce CJ, Bicanic N. A fully generalised, coupled, multi-phase, hygro-thermo-mechanical model for concrete. Mater Struct 2010;43(Suppl. 1).
[5] Mazars J, Pijaudiercabot G. Continuum damage theory – application to concrete. J Eng Mech – ASCE 1989;115(2):345–65.
[6] Davie CT, Pearce CJ, Bicanic N. Coupled heat and moisture transport in concrete at elevated temperatures – effects of capillary pressure and adsorbed water. Numer Heat Transfer, Part A 2006;49(8):733–63.
[7] Pearce CJ, Nielsen CV, Bicanic N. Gradient enhanced thermo-mechanical damage model for concrete at high temperatures including transient thermal creep. Int J Numer Anal Methods in Geomech 2004;28(7–8):715–35.
[8] Peerlings RHJ et al. Gradient-enhanced damage modelling of concrete fracture. Mech Cohesive-Friction Mater 1998;3(4):323–42.
[9] Stabler J. Computational modelling of thermo-mechanical damage and plasticity in concrete. Ph.D. Thesis, The University of Queensland, Australia; 2000.
[10] Gawin D, Pesavento F, Schrefler BA. Modelling of hygro-thermal behaviour of concrete at high temperature with thermo-chemical and mechanical material degradation. Comput Methods Appl Mech Eng 2003;192:1731–71.
[11] Davie CT, Zhang HL. Numerical investigation of damage and spalling in concrete exposed to fire. In: Computational modelling of concrete structures – EURO-C 2010. Rohrmoos/Schladming. Austria: Taylor & Francis Group; 2010.
[12] Zhang HL, Davie CT. A numerical investigation of the influence of pore pressures and thermally induced stresses for spalling of concrete exposed to elevated temperatures. Fire Safety J, submitted for publication.
[13] Kalifa P, Menneteau F-D, Quenard D. Spalling and pore pressure in HPC at high temperatures. Cement Concrete Res 2000;30:1915–27.
[14] Chung JH, Consolazio GR. Numerical modeling of transport phenomena in reinforced concrete exposed to elevated temperatures. Cement Concrete Res 2005;35:597–608.
[15] Pijaudier-Cabot G, Dufour F. Boundary and evolving boundary effects in non-local damage models. In: Computational modelling of concrete structures. EURO-C, Rohrmoos/Schladming. Austria: Balkema; 2010.
[16] Ramm E, Kato J. Material optimization for textile reinforced concrete applying a damage formulation. In: Computational modelling of concrete structures. EURO-C, Rohrmoos/Schladming. Austria: Balkema; 2010.
[17] Jirasek M, Horak M. Localization properties of damage models. In: Computational modelling of concrete structures. EURO-C, Rohrmoos/Schladming. Austria: Balkema; 2010.
[18] Mazars J et al. Fracture and compaction. In: Computational modelling of concrete structures. EURO-C, Rohrmoos/Schladming. Austria: Balkema; 2010.
[19] Giry C et al. Stress state influence on nonlocal interactions in damage modelling. In: Computational modelling of concrete structures. EURO-C, Rohrmoos/Schladming. Austria: Balkema; 2010.
[20] Pamin J, Winnicki A, Wosatko A. Simulations of dynamic failure in plain and reinforced concrete with regularized plasticity and damage models. In: Computational modelling of concrete structures. EURO-C, Rohrmoos/Schladming. Austria: Balkema; 2010.
[21] Wosatko A, Pamin J. Gradient damage model with volumetric–deviatoric split. In: Computational modelling of concrete structures. EURO-C, Rohrmoos/Schladming. Austria: Balkema; 2010.
[22] Marzec I, Tejchman J. Application of enhanced elasto-plastic damage models to concrete under quasi-static and dynamic cyclic loading. In: Computational modelling of concrete structures. EURO-C, Rohrmoos/Schladming. Austria: Balkema; 2010.
[23] Hertz KD. Limits of spalling of fire-exposed concrete. Fire Safety J 2003;38:103–16.
[24] Jansson R, Bostrom L. Spalling in concrete exposed to fire. 2008, SP Technical Research Institute of Sweden.
[25] Ali F, Nadjai A, Abu-Tair A. Explosive spalling of normal strength concrete slabs subjected to severe fire. Mater Struct 2011;44(5):943–56.
[26] Anderberg Y. Spalling phenomena of HPC and OC. In: Phan LT, et al., editor. International Workshop on Fire Performance of High-Strength Concrete Proceeding, NIST Special Publication 919, 1997, NIST, Gaithersburg, MD.
[27] C.-M. Aldea, J.-M. Franssen, J.-C. Dotreppe, Fire test on normal and high-strength reinforced concrete columns. In: Phan LT. et al., editor. International workshop on fire performance of high-strength concrete proceeding, NIST Special Publication 919, 1997, NIST, Gaithersburg, MD.
[28] Bailey C. Holistic behaviour of concrete buildings in fire. Proc Inst Civil Eng Struct Build 2002;152(3):199–212.
[29] Kodur V, McGrath R. Fire endurance of high strength concrete columns. Fire Technol 2003;39(1):73–87.
[30] Nielsen CV, Pearce CJ, Bicanic N. Theoretical model of high temperature effects on uniaxial concrete member under elastic restraint. Mag Concrete Res 2002;54(4):239–49.
[31] CEN, BS EN 1992-1-2:2004 Eurocode 2: Design of concrete structures – Part 1-2: General rules – Structural fire design. European Standards, London, 2004.
[32] de Borst R, Peeters P. Analysis of concrete structures under thermal loading. Comput Methods Appl Mech Eng 1989;77(3):293–310.

[33] Zeiml M, Lackner R, Mang HA. Experimental insight into spalling behavior of concrete tunnel linings under fire loading. Acta Geotech 2008;3(4): 295–308.
[34] Menou A et al. mortar and concrete subject to high temperature. Theor Appl Fract Mech 2006;45(1):64–71.
[35] Watanabe K, Bangi MR, Horiguchi T. Effect of elevated temperatures on flexural behaviour of hybrid fibre reinforced high strength concrete. J Struct Eng 2010;1(1):17–28.
[36] Fu YF, Li L. Study on mechanism of thermal spalling in concrete exposed to elevated temperatures. Mater Struct 2011;44(1):361–76.